GENETICS

Identification and characterization of the de novo methyltransferases for eukaryotic N^6-methyladenine (6mA)

Ting Cheng[1,2,3]†, Jiachen Zhang[1,2]†, Haicheng Li[1,2]†, Jinghan Diao[1,2]†, Wenxin Zhang[4], Junhua Niu[1,2], Takayuki Kawaguchi[3,5], Jun-ichi Nakayama[3,5], Kensuke Kataoka[3,5], Shan Gao[1,2]*

***N*^{6}-methyladenine (6mA) is an intensively investigated epigenetic modification in eukaryotes. 6mA is maintained through semiconservative transmission during DNA replication, but the identity of de novo methyltransferase (MTase) catalyzing its establishment remains unknown. Here, we identified MT-A70 family proteins AMT2 and AMT5 as the de novo MTases responsible for 6mA establishment, using the unique sexual reproduction process of the unicellular eukaryote *Tetrahymena thermophila*. Deletion of *AMT2* and *AMT5* led to a substantial decrease in 6mA levels in the progeny macronucleus, resulting in an altered gene expression pattern and a substantial decline in the survival rate of sexual progenies. Additionally, the maintenance MTase AMT1 could exhibit a much diminished de novo methylation activity in cells lacking AMT2 and AMT5. Our study delineated the establishment-maintenance pathway of 6mA and underscored the biological importance of de novo methylation, revealing a notable parallel between 6mA and the classical 5-methylcytosine in eukaryotes.**

INTRODUCTION

The last several years have witnessed an explosively increased research interest in eukaryotic DNA N^6-methyladenine (6mA) (*1*–*4*). As a potential epigenetic mark, 6mA plays important roles in various DNA and chromatin-based molecular pathways in eukaryotes, including transcription (both activation and repression), replication, DNA damage response, alternative splicing, and chromatin organization (*1*, *5*–*10*). It is also implicated in a plethora of physiological and pathological processes, including stress response, embryonic development, cellular physiology, plant growth and development, and tumor cell growth (*5*, *8*, *11*–*15*). Dissecting the molecular pathway for 6mA deposition in eukaryotes is critical for better understanding the 6mA biology.

The methylation pathway of the classical 5-methylcytosine (5mC) can be divided into two steps: establishment and maintenance. Establishment is conducted by the de novo methyltransferases (MTases) DNMT3A and DNMT3B (*16*), adding methyl groups to cytosines on unmethylated CpG dinucleotides. Maintenance is implemented by the maintenance MTase DNMT1 (*17*), which converts hemi-methylated CpG to full methylation, thus transmitting 5mC in a semiconservative manner and preventing its dilution by DNA replication (passive demethylation) (*18*). 5mC pattern is reset during mammalian embryonic development, with genome-wide active demethylation, followed by de novo methylation (*19*). Loss of *Dnmt3a*/*Dnmt3b* is embryonically lethal in mouse and has been linked with aberrant gene repression (*16*), underscoring the critical roles played by de novo DNA methylation.

We and others have previously identified the MT-A70 family protein AMT1 as the maintenance MTase, in the unicellular model eukaryote *Tetrahymena thermophila* (referred to as *Tetrahymena* hereafter) (*8*, *10*, *20*). 6mA occurs exclusively in the self-complementary ApT dinucleotides and can be maintained in a semiconservative way by AMT1 (*8*, *10*, *21*), providing definitive evidence to support 6mA as a bona fide epigenetic mark. However, it remains unclear which enzyme catalyzes the de novo 6mA deposition on unmethylated DNA. Intriguingly, there is still 6mA retained in Δ*AMT1* cells but, predominantly, in the form of hemi-6mApT, instead of full-6mApT as in wild-type (WT) cells (*8*, *21*), strongly suggesting the existence of de novo MTase activity. However, such de novo MTase activity is largely masked by the AMT1-dependent maintenance methylation in WT cells undergoing asexual reproduction by binary fission (referred to as vegetative growth) (*22*).

Tetrahymena provides a unique time window for the study of de novo 6mA. As featured for the binucleated ciliates, *Tetrahymena* contains two physically separate and functionally distinct nuclei (*23*–*25*). During the vegetative growth, 6mA only decorates the transcriptionally active macronucleus (MAC), but not the silent micronucleus (MIC) (*26*, *27*). This pattern is consistent with the association of 6mA with transcription, as also reported in basal fungi and algae (*1*, *28*). During the sexual reproduction (referred to as conjugation), 6mA pattern also needs to be reestablished. This process involves degradation of the somatic MAC, while the germline 6mA-free MIC gives rise to the 6mA-positive new MAC in progeny cells (Fig. 1A) (*29*), entailing de novo methylation of its genomic DNA. All the evidence strongly suggests that the methylation pathway for 6mA also features two distinct stages for establishment and maintenance.

In this study, we used the *Tetrahymena* new MAC that allows us to analyze de novo establishment and maintenance of 6mA separately. We systematically characterized AMT2 and AMT5, a pair of MT-A70 family proteins paralogous to AMT1 (Fig. 1B and table S1), as the candidate de novo 6mA MTases. We demonstrated that de novo 6mA in the new MAC was severely compromised in *AMT2*

[1]MOE Key Laboratory of Evolution & Marine Biodiversity and Institute of Evolution and Marine Biodiversity, Ocean University of China, Qingdao 266003, China. [2]Laboratory for Marine Biology and Biotechnology, Qingdao Marine Science and Technology Center, Qingdao 266237, China. [3]Division of Chromatin Regulation, National Institute for Basic Biology, Okazaki 444-8585, Japan. [4]Institute of Biomedical Research, Yunnan University, Kunming 650500, China. [5]The Graduate University for Advanced Studies, SOKENDAI, Okazaki 444-8585, Japan.
*Corresponding author. Email: shangao@ouc.edu.cn
†These authors contributed equally to this work.

and/or *AMT5* knockout (KO) cells. The substantial 6mA decrease, in turn, altered gene expression pattern and reduced the survival rate of sexual progenies, highlighting the importance of dedicated de novo MTase activity.

RESULTS

AMT2 and AMT5 are not required for the maintenance of 6mA

We previously demonstrated that 6mA level in the somatic MAC remained unaffected in *AMT2* and *AMT5* single KO cells during the vegetative growth (*8*). Here, we showed that 6mA level was not affected in double KO cells either (Fig. 2, A and B, and fig. S1). Consistent with our immunofluorescence (IF) and mass spectrometry (MS) results (*8*), Single Molecule Real-Time Circular Consensus Sequencing (SMRT CCS) further confirmed that neither the level nor the pattern of 6mA was altered in single or double KO cells during vegetative growth (Fig. 2, C and D, and table S2). This is most likely due to the fact that 6mA in WT *Tetrahymena* is almost exclusively at the ApT dinucleotides (6mApT/6mA > 99%) and mostly fully methylated (full-6mApT/6mApT > 88%) (*21*), which are efficiently maintained by the activity of AMT1 at this stage (*8*, *10*). In support of this dispensability, endogenously hemagglutinin (HA)–tagged AMT2 and AMT5 were undetectable in the somatic MAC

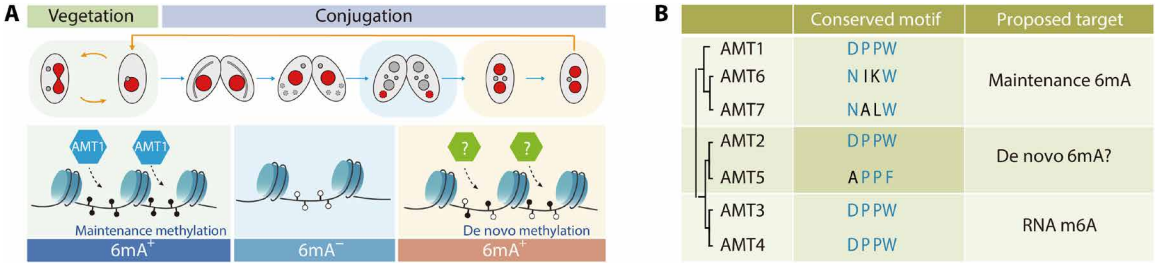

Fig. 1. 6mA dynamics and MT-A70 family MTases in *Tetrahymena*. (**A**) Top: Schematic drawing of nuclear events and 6mA distribution during vegetation and conjugation stages (red, 6mA positive; gray, 6mA negative). Bottom: Graphics of 6mA deposition by de novo and maintenance MTases. (**B**) Simplified phylogenetic tree of *Tetrahymena* MT-A70 family MTases, marked with their catalytic motifs and proposed functions.

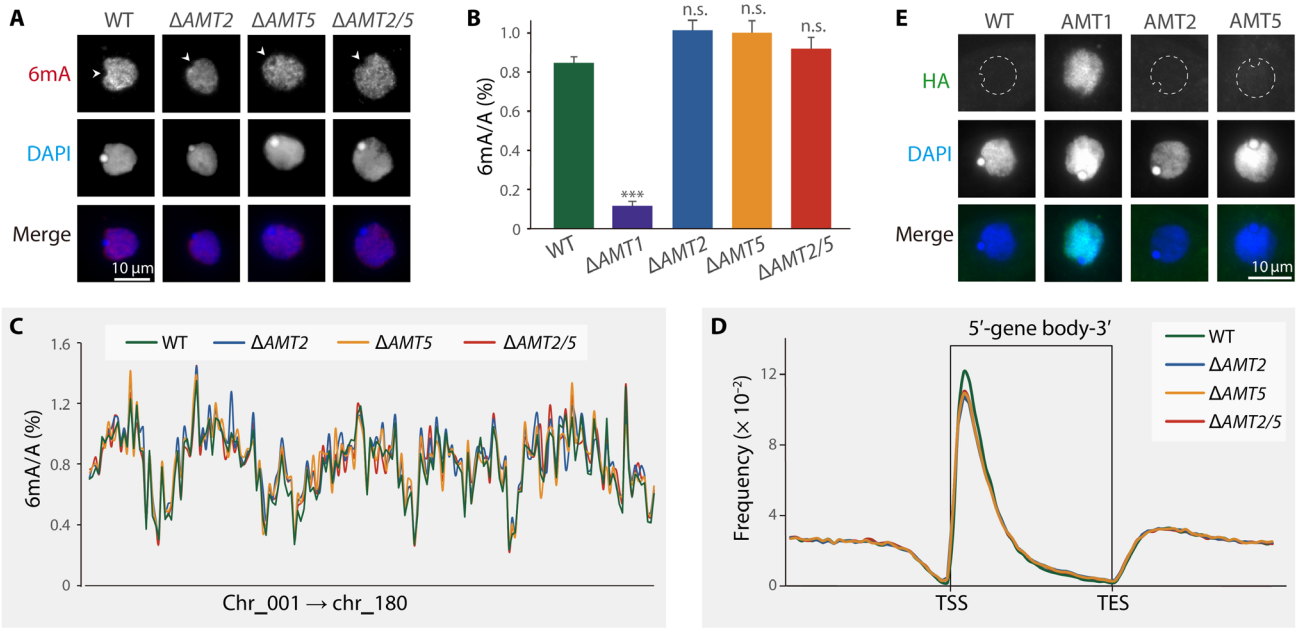

Fig. 2. AMT2 and AMT5 were not required for maintenance 6mA during the vegetative stage. (**A**) 6mA levels were not affected in the KO cells during the vegetative stage, as demonstrated by immunofluorescence (IF) staining. Arrowheads indicated the absence of 6mA signals in the MIC. (**B**) Mass spectrometry (MS) analysis revealed that 6mA levels in KO cells were not substantially changed during the vegetative growth. Δ*AMT1* strain was used as a control, showing a marked reduction in 6mA levels. Three biological replicates were conducted for each strain. ***$P < 0.001$; n.s., not significant ($P > 0.05$). (**C**) 6mA ratios, defined as the percentage of methylated adenines among all adenines (6mA/A), were comparable on 180 non-rDNA (nonribosomal DNA) MAC chromosomes between KO and WT cells during the vegetative stage. MAC chromosomes were arranged from left to right in accordance with their positions on the MIC chromosomes. (**D**) 6mApT dinucleotides were enriched toward the 5′ end of gene bodies in both KO and WT cells. Genes were scaled to unit length and were extended to each side by one unit length. One unit length was divided into 30 bins, and the distribution frequency was calculated as the ratio of the 6mA amount at each specific position to the total 6mA amount. TSS, transcription start site; TES, transcription end site. (**E**) IF staining showed that AMT2 and AMT5 were not detectable in the somatic MAC (dashed circles) of vegetative cells. Hemagglutinin (HA)–tagged AMT1 cells and WT (SB210) cells without the HA tag were used as positive and negative controls, respectively.

during the vegetative growth (Fig. 2E); however, they were detected during conjugation (the sexual stage of ciliates) (Fig. 3B and fig. S2), thus ruling out the possibility of HA tagging failure. Consistently, the growth rate of vegetative cells was comparable in WT and KO cells (fig. S3). Together, our results demonstrated that AMT2 and AMT5 are not required for maintenance 6mA in the somatic MAC.

AMT2 and AMT5 are required for de novo 6mA

To determine whether AMT2 and AMT5 are responsible for de novo 6mA methylation, we first examined their expression patterns. Both *AMT2* and *AMT5* showed a two-peak profile: one at early conjugation and the other at late conjugation corresponding to the stage of new MAC development (Fig. 3A) (*30*). Consistent with their expression profiles, the endogenously tagged AMT2 and AMT5 first localized in the parental MAC and then in the newly formed MACs (Fig. 3B and fig. S2).

During the stage of new MAC development, 6mA in WT cells exclusively occurred in the new MACs of exconjugants (when the two progenies separate) (Fig. 1A). In MAC KO cells, which lacked the maternal transcripts of *AMT2* and *AMT5*, 6mA signals remained unchanged (Fig. 3C). Similarly, 6mA signal intensity was not affected in MIC KO cells with the exclusive absence of the zygotic transcripts (Fig. 3C). It is only in complete KO cells, where both maternal and zygotic transcripts were eliminated, that 6mA signals become undetectable (Fig. 3C). This marked reduction of 6mA was corroborated by the MS analysis conducted on flow cytometry–purified new MACs of complete KO cells (Fig. 3D). We therefore conclude that the deposition of de novo 6mA is attributable to both maternally and zygotically expressed AMT2 and AMT5.

To test whether the 6mA absence in the new MAC was solely attributable to the lack of *AMT2* or *AMT5*, we introduced WT *AMT2* or *AMT5* to their endogenous MAC locus of corresponding KO cells (fig. S5, A, B, E, and F). Western blot analysis confirmed that AMT2 and AMT5 were restored to WT levels in rescued cells (fig. S5, C and G). Moreover, 6mA signal intensity was restored (Fig. 3E and fig. S5H).

AMT2 featured the conserved catalytic motif DPPW ([DNSH]PP[YFW]), while AMT5 contained the eroded APPF (Fig. 3F and fig. S6) (*8*, *31*). To determine whether the intrinsic enzymatic activity of AMT2 underpinned its function, we carried out the rescue experiment by introducing the catalytically inactive AMT2 (APPA or APPF as in AMT5) back into Δ*AMT2* cells (fig. S5, A and D). Neither APPA nor APPF was able to restore 6mA levels (Fig. 3E and fig. S5H), suggesting that the AMT2 catalytic activity is required for 6mA methylation.

Next, we tested the physiological consequences that may result from the deficiency of 6mA. We found that the conjugation progress was delayed in cells lacking *AMT2* and/or *AMT5* compared to WT cells, especially during 10 to 14 hours post-mixing (Fig. 3G). Although such delays could be subsequently mitigated, possibly due to the compensational effect of AMT1 (*8*), viability rates of KO progenies were substantially lower than WT counterparts (Fig. 3H, fig. S7, A and B, and table S3), underscoring the functional significance of AMT2/AMT5 and de novo 6mA for conjugation progression and progeny development. Moreover, the conjugation delay and progeny mortality suffered by the Δ*AMT2* cells could be partially alleviated by the WT copy of AMT2, but not by the APPA copy (fig. S7, C and D), indicating that the observed defects are due to the impaired enzymatic function of AMT2.

It should be noted that we observed no synergistic or additive effect for the double KO of *AMT2* and *AMT5*, compared to single KO. Moreover, the global transcription profiles of the conjugation progenies for single and double KO cells were more similar to each other than to WT control cells (fig. S8), strongly indicating that AMT2 and AMT5 function cooperatively rather than independently. However, AMT2 and AMT5 alone exhibited no MTase activity in vitro and in vivo (fig. S9), consistent with the necessity of additional cofactors for the DNA 6mA MTase activity in the MT-A70 family (*10*, *32*). Together, these results strongly argued that AMT2 and AMT5 are essential for the de novo establishment of 6mA in the new MAC, as well as for the cell fitness.

6mA landscapes are similar between the WT new MAC and the WT somatic MAC

To further explore the 6mA pattern change, we performed SMRT CCS of flow cytometry–purified new MACs from both WT and KO cells. After applying a stringent threshold and filtering out abnormal DNA molecules (see more details in Methods and Materials), 1,627,095, 1,874,423, 1,974,209, and 1,153,747 high-confidence single molecules for WT, Δ*AMT2*, Δ*AMT5*, and Δ*AMT2/5* cells, respectively, were used for further analysis (table S4).

We first performed a comparative analysis between WT new MAC (WT) and WT somatic MAC (WT-veg) (*21*). 6mA exhibited notable similarities in these two stages. (i) 6mA occurred almost exclusively at the ApT dinucleotides in the new MAC (6mApT/6mA > 99%), consistent with the somatic MAC (>99%) (figs. S10A and S11A). 6mA in non-ApT dinucleotides (ApC/ApG/ApA) was called at low levels close to the background noise using the same threshold (figs. S10A and S11B). (ii) 6mApT represented 2.25% of all mapped ApT sites (6mApT/ApT) (versus 2.03% in the somatic MAC) (Table 1). Correspondingly, 6mA level (6mA/A) was comparable between two samples (0.82% in the new MAC versus 0.74% in the somatic MAC) (Table 1). (iii) There were substantial overlaps in 6mApT positions between new MAC and somatic MAC; most ApT positions methylated in the somatic MAC were also methylated in the new MAC (fig. S10B). When 6mApT positions were divided into 10 quantiles according to their penetrance (ratio between the number of 6mA sites and all adenine sites in all SMRT CCS reads) in the somatic MAC, 6mApT in the new MAC displayed a similar distribution in each quantile; sites of high penetrance in the somatic MAC had a higher tendency to be also highly methylated in the new MAC (fig. S10C). (iv) 6mA in both samples were enriched at gene bodies, toward the 5′ end and downstream of the transcription start sites (fig. S10D) (*8*, *27*). (v) 6mA levels at individual genes showed strong correlation between the new MAC and the somatic MAC (fig. S10E; Spearman's correlation coefficient = 0.93, $k = 0.99$). Collectively, these connections matched with the scenario that 6mA landscape was nearly established in the new MAC, before cells reentered the vegetative growth stage (*29*).

Despite these connections, there were distinctions between 6mA in the new MAC and the somatic MAC. First, the percentage of fully methylated 6mA was lower in the new MAC than in the somatic MAC (75.21% versus 88.35%) (Table 1), a phenomenon commonly observed at the individual single-molecule level (fig. S10F). This might be partially attributable to the low activity of AMT1 during the new MAC development (*8*). Second, some highly methylated sites in the new MAC were not transmitted and maintained

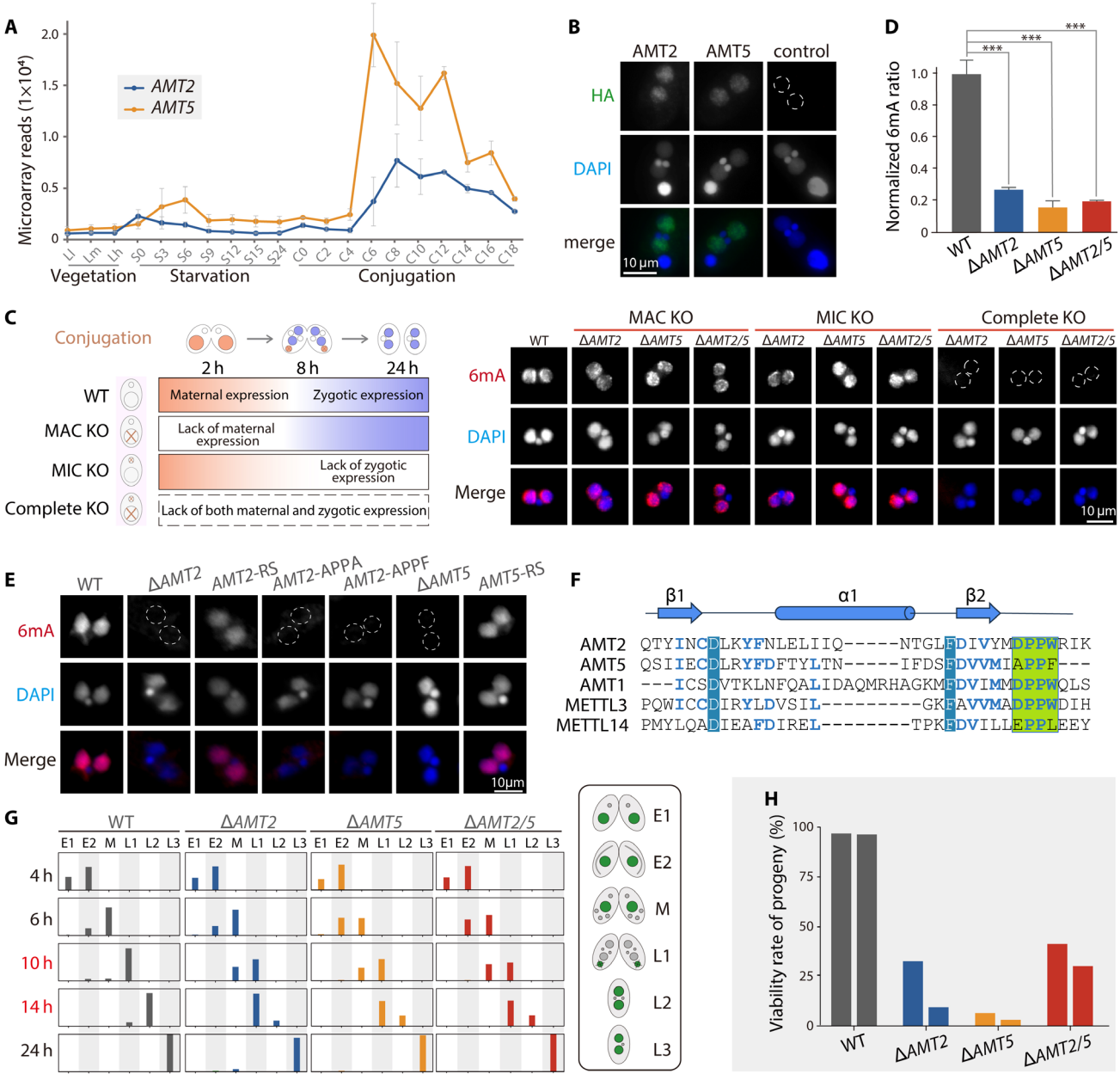

Fig. 3. AMT2 and AMT5 were essential for de novo 6mA during the conjugation stage. (**A**) *AMT2* and *AMT5* are highly expressed during new MAC formation of conjugation stage (*30*). (**B**) AMT2 and AMT5 were localized in the newly formed MAC. Note the absence of the HA signal in the new MAC (dashed circle) of WT control cells. (**C**) Both somatically and zygotically expressed AMT2 and AMT5 contributed to de novo 6mA deposition. Left: Expression pattern of maternal and zygotic *AMT2* and *AMT5* in WT and KO cells. Right: 6mA signals in the new MAC of MAC KO (no maternal expression), MIC KO (no zygotic expression), and complete KO cells. Note the absence of 6mA signals in the new MAC (dashed circles) of complete KO cells. (**D**) MS analysis of 6mA levels in the flow cytometry–purified new MAC. Three biological replicates for each strain. ***$P < 0.001$. (**E**) IF staining analysis of 6mA levels in the new MAC. The outline of the nuclei without 6mA signals was delineated with dashed circles. (**F**) Alignment of sequences surrounding the catalytic motif in AMT1, AMT2, and AMT5 of *Tetrahymena* and in human METTL3 and METTL14. Identical sequences were indicated by white letters with blue background, while similar sequences were indicated by bold blue letters. The DPPW catalytic motif was depicted with a green background. (**G**) Conjugation progress of KO and WT cells. The schematic on the right illustrated the corresponding nuclear morphologies at each stage. E1, pre-meiosis; E2, meiosis, M, mitosis; L1, new MAC development, L2, pair separation; L3, one of the new MIC degraded. $n > 200$ for each strain. *n* represents the number of single cells. h, hours. (**H**) The viability rate of KO and WT progenies. Two biological replicates for each strain.

Table 1. SMRT CCS results for the flow cytometry–purified new MAC at 24 hours post-mixing during conjugation.

	Single molecule	A sites	6mA sites	ApT sites	6mApT sites	Full	Hemi-C	Hemi-W	Total 6mApT
WT	Number	2,650,998,266	21,821,071	917,555,698	20,651,604	15,531,852	2,569,180	2,550,572	20,651,604
	Percentage (%)	–	0.82	–	2.25	75.21	12.44	12.35	–
Δ*AMT2*	Number	4,562,894,840	5,524,473	1,573,597,700	4,750,706	3,828,384	461,348	460,974	4,750,706
	Percentage (%)	–	0.12	–	0.30	80.59	9.71	9.70	–
Δ*AMT5*	Number	4,138,411,182	4,296,775	1,429,134,888	3,502,851	2,758,540	372,416	371,895	3,502,851
	Percentage (%)	–	0.10	–	0.25	78.75	10.63	10.62	–
Δ*AMT2/5*	Number	2,963,324,787	3,977,697	1,021,233,408	3,275,705	2,623,536	326,384	325,785	3,275,705
	Percentage (%)	–	0.13	–	0.32	80.09	9.96	9.95	–
WT-veg*	Number	2,430,618,393	17,889,360	823,903,428	16,765,614	14,811,496	974,677	979,261	16,765,614
	Percentage (%)	–	0.74	–	2.03	88.35	5.81	5.84	–
Δ*AMT1*-veg*	Number	1,730,640,574	3,443,531	645,000,722	3,420,511	82,362	1,670,284	1,667,685	3,420,511
	Percentage (%)	–	0.20	–	0.53	2.40	48.83	48.77	–

*Data from Sheng *et al*. (*21*).

in the somatic MAC (fig. S10C), which were likely to be independent of AMT1.

AMT2 and AMT5 are required for the proper establishment of the 6mA landscape

Compared to WT cells, 6mApT/ApT ratio in the new MAC was markedly reduced to 0.30, 0.25, and 0.32% in Δ*AMT2*, Δ*AMT5*, and Δ*AMT2/5* cells, respectively (Table 1). Correspondingly, 6mA level (6mA/A) in KO cells was lower than that in WT cells in all 180 non-rDNA (nonribosomal DNA) chromosomes (0.12, 0.10, and 0.13% in Δ*AMT2*, Δ*AMT5*, and Δ*AMT2/5* versus 0.82% in WT cells) (Fig. 4A and Table 1), consistent with the IF staining and MS results (Fig. 3, C and D). This reduction is even more marked than vegetative cells depleting *AMT1* (Δ*AMT1*, 6mA/A = 0.20%) (*8*, *21*).

Many ApT positions were methylated in WT cells but not in Δ*AMT2*, Δ*AMT5*, and Δ*AMT2/5* cells (Fig. 5), with only a small proportion of overlapped sites (9.26, 4.11, and 3.74% of WT 6mApT sites) (Fig. 6A and fig. S12A). Along with the global reduction of methylated 6mA sites (Fig. 4A and Table 1), the penetrance of individual 6mA sites was generally much lower in KO cells; 6mA positions of high penetrance were especially depleted (Figs. 4B and 5). At individual genes, 6mA levels were also substantially reduced, more marked than in Δ*AMT1* cells (Fig. 4C). Together, these results strongly argued for the essential role of AMT2 and AMT5 to establish the proper 6mA landscape in the new MAC.

To interrogate the features of AMT2/AMT5-deposited 6mA more directly, we first selected 6mA sites remaining in vegetative Δ*AMT1* cells that were presumably methylated by AMT2 and AMT5 (*21*). Intriguingly, 90.4% of these sites were unmethylated in the new MAC of cells lacking *AMT2* and *AMT5* (Fig. 4D). Next, to minimize the effect of AMT1, we focused on sites displaying comparable penetrance in WT (WT-veg) and in Δ*AMT1* cells (Δ*AMT1*-veg) (Fig. 4E) (*21*). These identified sites were designated as AMT1 independent, enabling a targeted evaluation of their reliance on AMT2 and AMT5. Penetrance of these selected sites was substantially lower in KO cells compared to WT cells, consistent with the trend observed at other sites (Fig. 4E). Their penetrance was much more diminished to zero in KO cells than the rest sites (Fig. 4E), highlighting the important contribution of AMT2 and AMT5 in their modification. Given that these sites are predominantly in hemi-methylated state in Δ*AMT1* cells (*21*), we postulated that AMT2/AMT5-deposited 6mA is hemi-methylated.

AMT1 catalyzes 6mA deposition in the new MAC without AMT2/AMT5

Albeit at a notably lower level (Figs. 4B and 5), the vast majority of remaining 6mA sites in the new MAC of KO cells were also methylated in WT cells (Fig. 6A and fig. S12A). The methylation pattern of these remaining 6mA in KO cells was reminiscent of that in WT cells; they still occurred at the ApT dinucleotides toward the 5′ end of the gene body (Figs. 5 and 6, B and C) (*8*). Moreover, the full/hemi ratio (defined as ratio between full-6mApT and hemi-6mApT) in KO cells remained similar to that in WT cells (fig. S11C and Table 1). Full-6mApT in KO cells was likely not generated by the random combination of two independent hemi-methylation events, as the penetrance strand bias of 6mA in KO cells converged to zero along with the increase of 6mA coverage (fig. S11D) (*21*).

The similar 6mA pattern in the new MAC of both WT and KO cells was presumably the product of AMT1. We favored the scenario that, in the absence of AMT2 and AMT5, AMT1 catalyzed de novo methylation on a limited number of ApT sites and converted a large majority of them into full methylation (*21*). AMT1 was localized into the new MAC (*8*) and its protein level in the new MAC was comparatively lower than in the somatic MAC of conjugation progenies after refeeding (Fig. 6D), partially explaining the lower full/hemi ratio in the new MAC (Table 1). We also noticed that AMT1

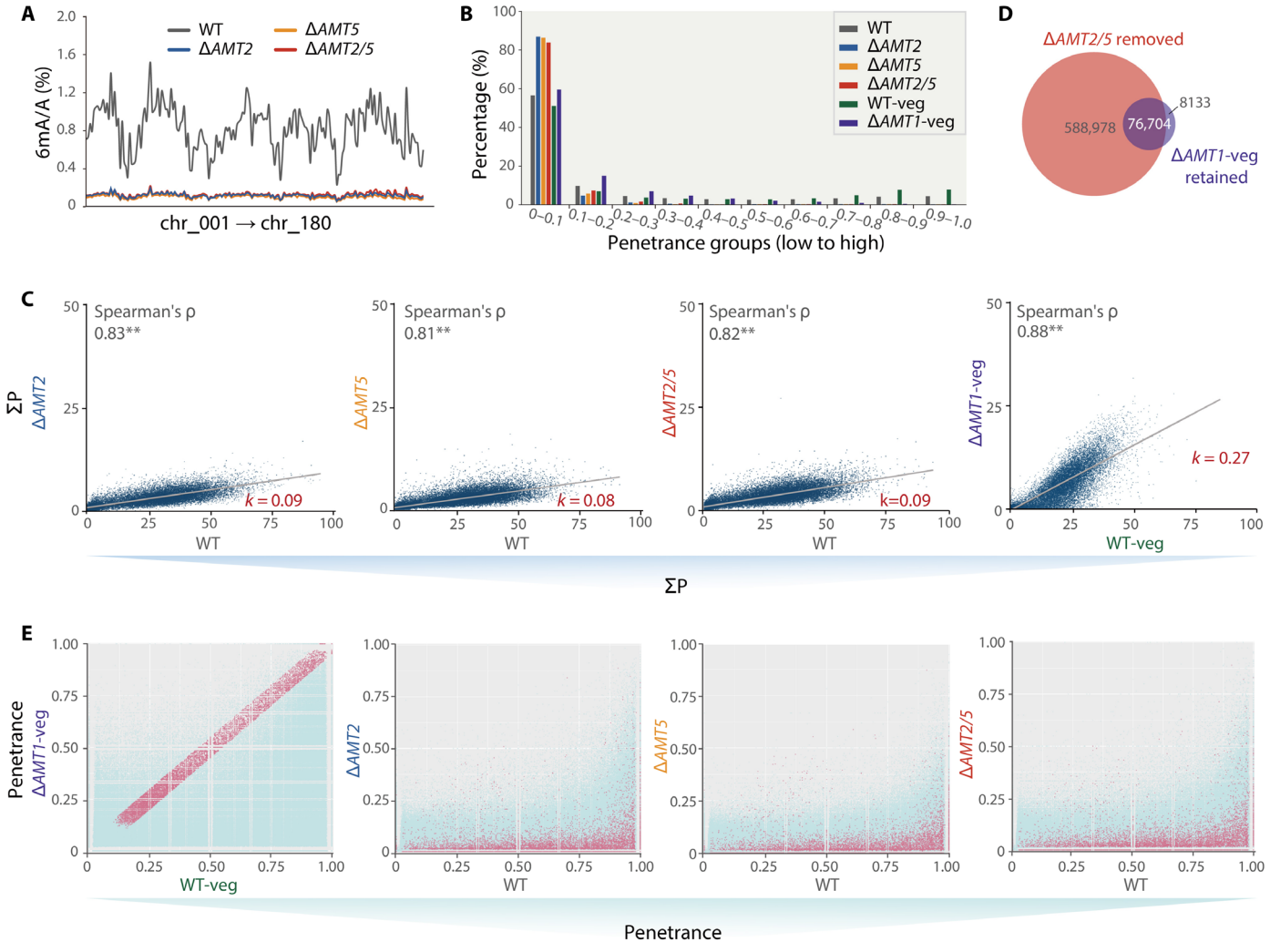

Fig. 4. 6mA establishment was severely impaired in the new MAC of *AMT2* and/or *AMT5* KO cells. (**A**) 6mA ratios exhibited a global decrease across all 180 non-rDNA chromosomes in KO cells at 24 hours post-mixing. Chromosome numbering followed the assignment outlined by Sheng *et al.* (*65*). (**B**) 6mApT positions with high penetrance in the new MAC of WT cells were depleted in KO cells. 6mApT positions were divided into 10 groups according to their penetrance, from low to high. 6mA SMRT-CCS data from the somatic MAC of Δ*AMT1* (Δ*AMT1*-veg) and WT (WT-veg) cells were included for comparison. (**C**) 6mA levels of individual genes were markedly reduced in the new MAC of KO cells, as well as in Δ*AMT1*-veg. 6mA level was calculated as "the sum of penetrance of all 6mApT positions (ΣP) on a specific gene." (**D**) Venn diagram illustrated that the vast majority of the retained 6mA sites in Δ*AMT1* cells were unmethylated in the new MAC of Δ*AMT2/5* cells. Δ*AMT2/5* removed sites were as defined as "positions with less than 10× coverage of 6mApT in the new MAC of Δ*AMT2/5* cells." Δ*AMT1*-veg retained sites were defined as "positions with more than 10× coverage of 6mApT in the somatic MAC of Δ*AMT1* cells." (**E**) The penetrance of AMT1-independent 6mApT positions was more substantially reduced in Δ*AMT2/5* cells. AMT1-independent 6mApT positions, depicted as red points, were defined as having a penetrance difference ≤ ±0.05 between WT-veg and Δ*AMT1*-veg, with 6mApT coverage ≥ 5× in both strains. The reduction in penetrance of AMT1-independent 6mApT positions was more pronounced than the rest majority of 6mApT positions in the new MAC of KO cells.

protein level was up-regulated in KO cells than in WT cells during late conjugation and after refeeding (Fig. 6D), which presumably contributed to 6mA recovery (Fig. 6E).

To monitor the 6mA recovery, we introduced an HA tag to the endogenous *RPB3* locus in the somatic MAC, to distinguish true progeny (HA negative, somatic MAC degraded) from non-maters and quitters (HA positive, somatic MAC retained) (Fig. 6E, left). In the presence of AMT1, 6mA level in progenies of KO cells could be restored to that of WT cells (Fig. 6E, right), at as early as 10 hours after refeeding (fig. S12B). MS analysis also showed that 6mA level in the conjugation progenies of KO cells was comparable to that in their WT counterparts (Fig. 6F).

DISCUSSION

AMT2 and AMT5 are de novo 6mA methyltransferases

We and others have demonstrated that AMT1 functioned as the maintenance MTase, displaying a higher enzymatic activity toward the hemi-methylated ApT than unmethylated ApT (*8*, *10*, *21*). Notably, AMT1 also had a comparatively lower de novo MTase activity, being able to catalyze methylation on unmethylated substrates, demonstrated by in vitro assay (*10*, *21*). However, when Δ*AMT1* cells mated with one another, the majority of mating pairs could not progress to the new MAC stage (*8*), thus constraining our capacity to investigate the de novo deposition of 6mA during new MAC formation. Nevertheless, among the rare Δ*AMT1* survivors that

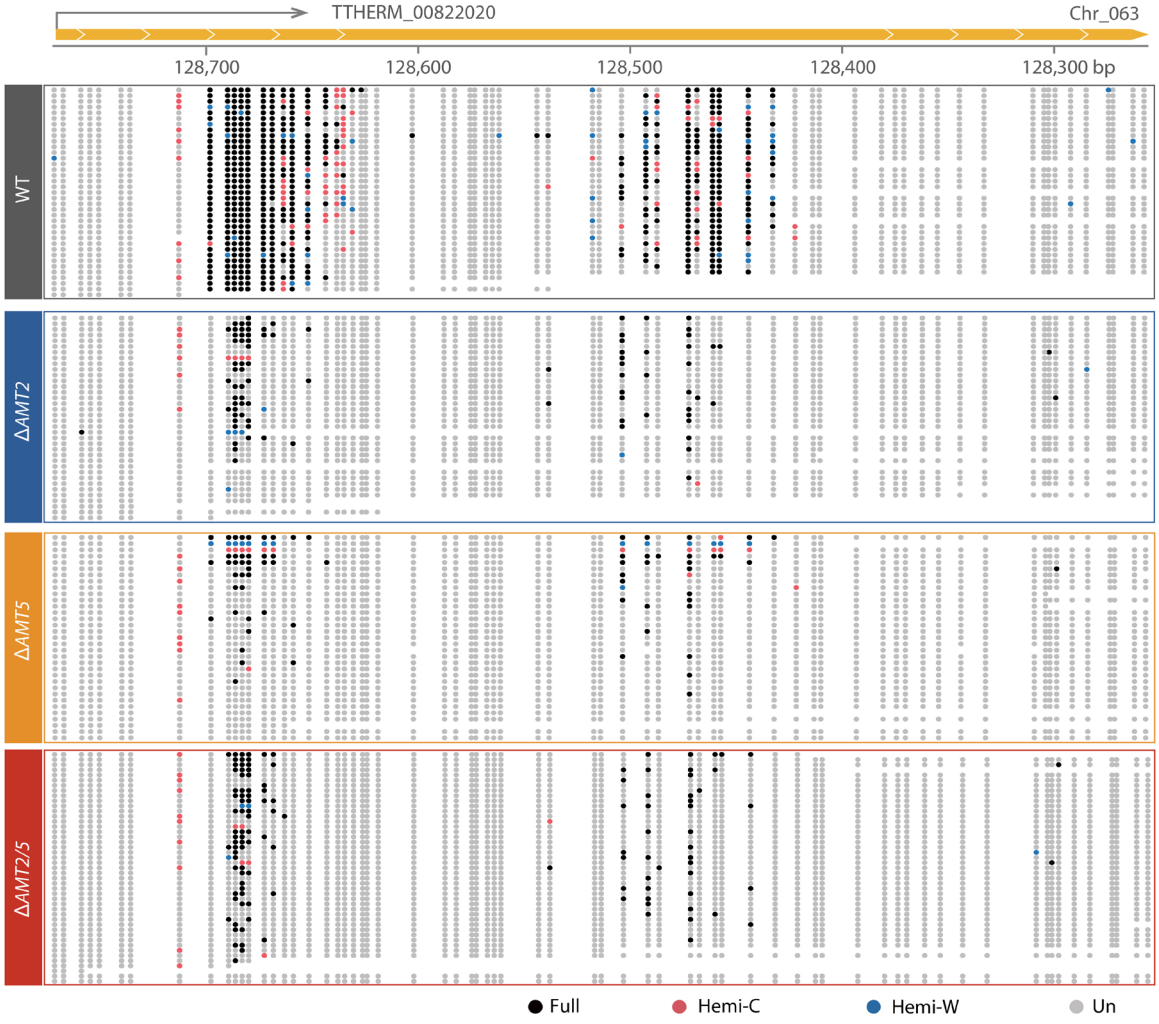

Fig. 5. Typical DNA single molecules revealed that a substantial proportion of highly methylated 6mApT sites in WT cells were either unmethylated or lowly methylated in KO cells. The methylation states of a self-complementary ApT duplex were divided into four categories: full (methylation on both Watson and Crick strands, black dots), hemi-C (methylation only on the Crick strand, red dots), hemi-W (methylation only on the Watson strand, blue dots), and un (no methylation, gray dots). bp, base pairs.

succeeded to enter the new MAC stage, *AMT1* deletion caused marked 6mA hypomethylation but not a complete loss (*8*). This observation strongly suggests the involvement of alternative MTases in de novo 6mA deposition (*8*, *10*, *21*).

Previous works have assigned seven members of the *Tetrahymena* MT-A70 family MTases (AMTs1-7) into different functional groups (*8*). Among them, AMT6 and AMT7 are partners of AMT1, while AMT3 and AMT4 catalyze RNA methylation (m6A) (*8*, *10*, *21*, *31*). As no additional MTases are known at present for *Tetrahymena*, it leaves AMT2 and AMT5, which group on the same subclade of the MT-A70 protein phylogenetic tree (*8*), as the candidates for de novo 6mA MTases.

In this study, we demonstrated that KO of *AMT2* and/or *AMT5* not only abolished methylation on a large majority of ApT sites but also attenuated the methylated ApT sites to reach high penetrance. The marked 6mA decrease, in turn, had a profound impact on the survival of conjugation progenies. The features of AMT2/AMT5-catalyzed 6mA could be partially deduced from the remaining sites in Δ*AMT1* cells, with the preferential accumulation on ApT dinucleotides, the 5′ end of gene body, and linker DNA regions, and in hemi-methylated forms (*8*, *21*).

In WT cells, the establishment of 6mA landscape during late conjugation was the coordinated work of AMT2/AMT5 and AMT1 (Fig. 7A). During the transition from 6mA-free zygotic MIC to 6mA-positive new MAC (*29*), AMT2 and AMT5 catalyzed unmethylated adenines into hemi-6mA, which was further converted into full-6mA by AMT1. In *AMT2* and/or *AMT5* KO cells, however, the impaired un-to-full conversion became the limiting step for AMT1 function. Instead, AMT1 conducted a two-step catalyzation on its own: un-to-hemi and then hemi-to-full. The former reaction was not effective enough, with only 10 to 20% of WT 6mApT sites being methylated at low penetrance, highlighting the indispensability of AMT2 and AMT5 for the establishment of proper 6mA landscape. It also provided strong in vivo evidence for the ability of AMT1 to target unmethylated DNA. The latter reaction was comparatively efficient, resulting in the typical footprint of AMT1 such as

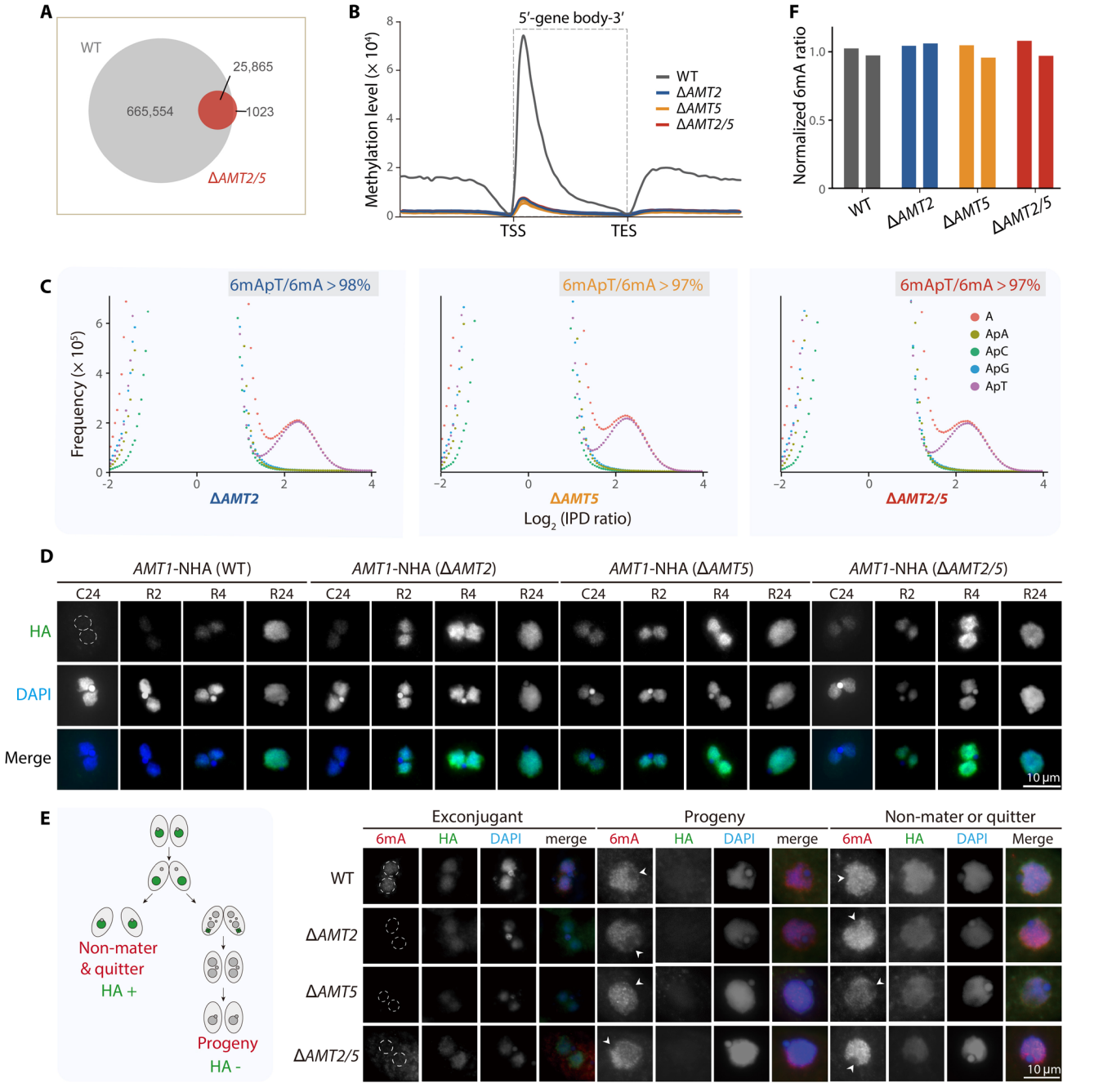

Fig. 6. The methylation pattern of the remaining 6mA sites in the new MAC of KO cells was attributed to AMT1. (**A**) Venn diagram illustrated the overlap between methylated 6mA sites in the new MAC of WT and Δ*AMT2/5* cells. The same cutoff (6mApT coverage ≥ 10×) was applied to both samples. (**B**) 6mApT exhibited an enrichment toward the 5′ end of gene bodies in both KO and WT cells. Genes were scaled to a unit length and were extended by one unit length on each side. One unit length was divided into 30 bins, and the sum of penetrance within each bin represented the methylation level. (**C**) 6mA displayed a preference for ApT dinucleotides in KO cells. Note that the bimodal distributions of both adenines (A) and ApT dinucleotides (ApT) were less obvious in KO cells than in WT cells (fig. S11A), due to the highly reduced number of 6mApT sites. (**D**) AMT1 levels were up-regulated in KO cells both at late conjugation and after refeeding. AMT1 was N-terminally HA-tagged in both MAC and MIC endogenous loci. New MACs without the HA signal were delineated with dashed circles. C24: 24 hours post-mixing. R2, R4, and R24: 2, 4, and 24 hours after refeeding. (**E**) 6mA signal intensity was restored in KO progenies. Left: Schematic diagram showing that the *RPB3*-CHA construct was transformed into somatic MACs to distinguish progeny (HA negative) from non-mater or quitter (HA positive). Right: 6mA occurrence in KO exconjugants before refeeding was abolished but was restored after refeeding (progeny). New MACs of the exconjugants were circled with white dashed lines, and the arrowheads indicated the absence of 6mA signals in MICs. (**F**) MS analysis of 6mA levels in KO and WT progenies. Two biological replicates for each strain.

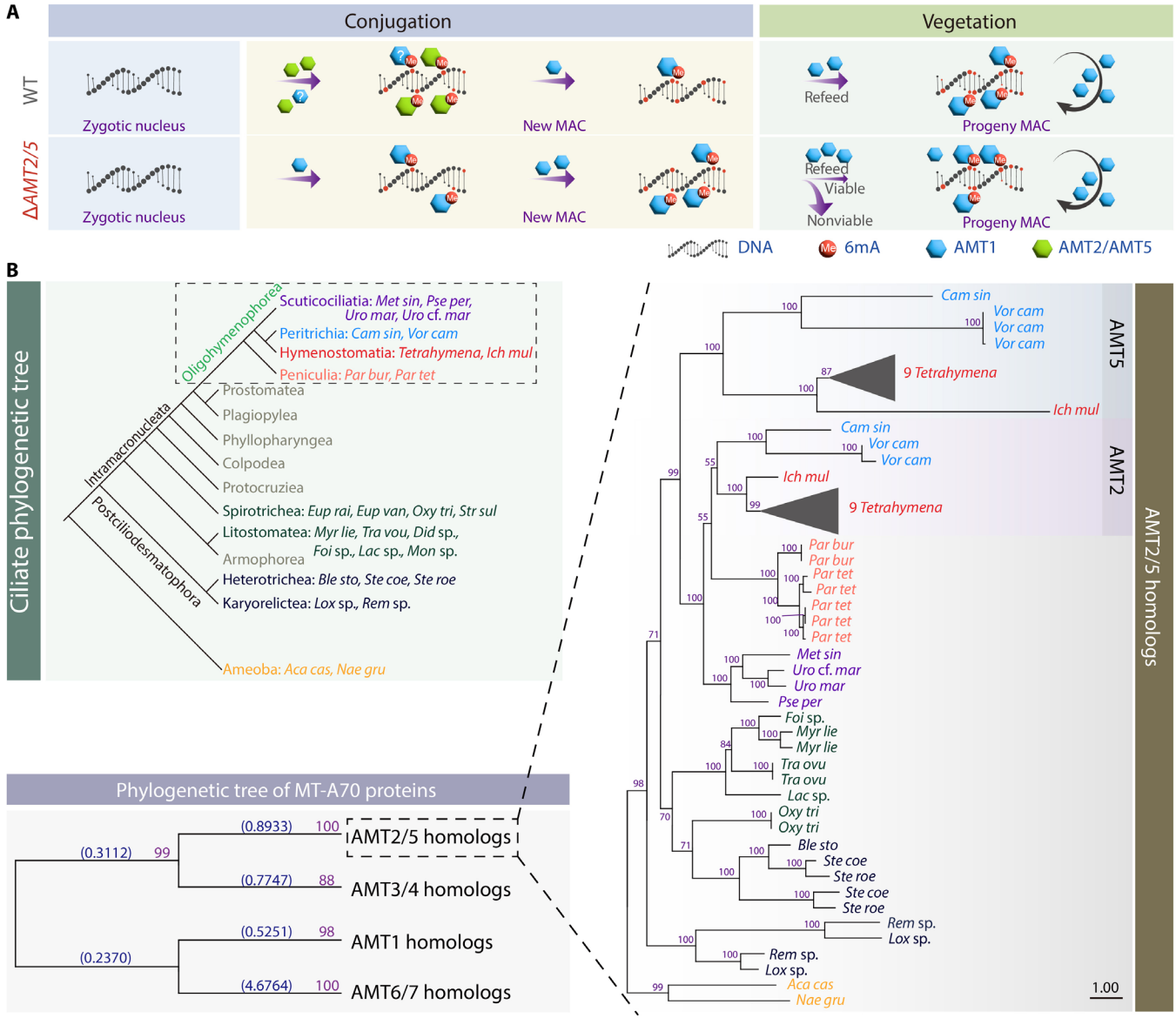

Fig. 7. Proposed regulatory model for 6mA and phylogenetic analysis of AMT2 and AMT5 homologs in ciliates. (**A**) A proposed model for 6mA establishment and maintenance in WT and KO cells. In the new MAC of WT cells, AMT2 and AMT5 initiated the de novo 6mA deposition on unmethylated ApT dinucleotides, possibly helped by AMT1, generating hemi-6mApT. Subsequently, these hemi-6mApT sites were converted into full-6mApT by the maintenance activity of AMT1. In the somatic MAC of progenies during the vegetative stage, established full-6mApT sites were faithfully maintained by AMT1. In *AMT2* and/or *AMT5* KO cells, however, the deposition of de novo 6mA dependent on AMT2 and AMT5 was abolished, while AMT1 could exhibit both de novo and maintenance activities and generate both hemi- and full-6mA on a limited number of sites. After refeeding, 6mA levels in KO cells could be restored to that of WT cells, probably owing to the up-regulated level of AMT1. (**B**) Phylogenetic analysis showed the divergence of AMT2 and/or AMT5 homologs in ciliates. Proteins were labeled by species abbreviations and colored on the basis of their phylogenetic positions in the ciliate phylogenetic tree (inset). Phylogenetic analysis of MT-A70 family proteins (homologs of AMT1, AMT2/AMT5, AMT3/AMT4, and AMT6/AMT7) was shown as the evolutionary tree in the lower left corner. The homologs of AMT2 and AMT5 were shown in detail on the right, and homologs of nine *Tetrahymena* species were represented by black triangles. The scale bar corresponds to 1 expected amino acid substitution per site. Species abbreviations and NCBI GI numbers were listed in file S1.

the predominance of full-6mA and the enrichment at the 5′ end of gene bodies (*8*, *21*, *27*). It also suggested that AMT1, or even AMT2 and AMT5, is interacting with other epigenetic factors during new MAC development, to achieve their genomic targeting. Those factors could be H3K4me3 and H2A.Z, as demonstrated in vegetative cells (*8*, *27*), which are already abundant in the new MAC at this stage (*33*, *34*).

In *AMT2* and/or *AMT5* KO cells, the occurrence of 6mA was not recovered until refeeding. During the late stage of conjugation without refeeding, AMT1 activity likely remained low, modulated by both its low protein level and the possible absence or low levels of its interacting proteins. After refeeding, however, AMT1 level was markedly up-regulated, probably for fulfilling its role as a maintenance MTase (*21*). The elevated level of AMT1 successfully restored

global 6mA levels in KO cells to that of WT cells, although we could not rule out the possibility that a small proportion of sites that relied solely on AMT2/AMT5 might remain unmethylated. Given that very few (endo)replication was observed during late conjugation (fig. S12C) (*35*), in contrast to active replication during the vegetative stage (*36*), we speculated that AMT1 level and/or activity might also be linked with replication.

Together, our work identified and characterized the de novo MTases for eukaryotic 6mA, affirming the long-standing hypothesis that 6mA dynamics also involve a two-step pathway. These findings, combined with our previous discoveries regarding AMT1, delineate a detailed pathway for the proper establishment and maintenance of 6mA. However, no physical interaction was detected between AMT1 and AMT2/AMT5 (fig. S13), arguing against the possibility of a super-complex.

Evolution of AMT2 and AMT5, with speculations on their interactions

Previous studies assigned AMT2 and AMT5 into the same phyletic subclade of the MT-A70 family MTases (*8*, *31*). Further analysis revealed that orthologs of AMT2 and AMT5 are not universally distributed in unicellular eukaryotes (Fig. 7B), unlike AMT1, AMT6, and AMT7 (*8*). Instead, they are mostly exclusively present in ciliates. This coincides with the unique nuclear dualism in these organisms and massive genome-wide de novo 6mA deposition during MIC-to-MAC differentiation, thus providing the new perspective on the distinct evolution of ciliates through the lens of 6mA methylation.

Orthologs of AMT2 and AMT5 are present in both ciliate subphylums Postciliodesmatophora and Intramacronucleata and in 5 classes with reported genomes, so far, of the 11 ciliate classes (Fig. 7B) (*37*). However, only in two (Hymenostomatia and Peritrichia) of the seven subclasses in the class Oligohymenophorea, namely, species of *Tetrahymena* and their very close relatives like *Ichthyophthirius multifiliis*, which is a pathogen causing white spot disease in fish, are there two paralogues equivalent to AMT2 and AMT5 (Fig. 7B).

The divergence of AMT2 and AMT5 probably occurred after the separation of *Tetrahymena* and *Paramecium* around 750 million years ago (*38*), as *Paramecium* contained only homologs of AMT2 (Fig. 7B). This late gene duplication event within a small group of ciliates is compatible with two scenarios: either AMT2 and AMT5 function separately or they form a heterodimer complex in *Tetrahymena* and its close relatives. Our current results lend stronger support to the latter scenario on several aspects. First, both the catalytic motif and the SAM-binding key residues were only conserved in AMT2 (DPPW and FxR, respectively), but not in AMT5 (APPF and FTK) (*39*–*41*). Meanwhile, most of other residues contributing to SAM or DNA binding in the AMT1 complex were conserved in AMT2 but not in AMT5 (fig. S6) (*39*–*41*). It was therefore required for AMT5 to dimerize with AMT2 for activity. Second, we observed no synergistic or additive effect for the double KO of *AMT2* and *AMT5*, strongly indicating that AMT2 and AMT5 function cooperatively rather than independently. In further favor of the heterodimer scenario, members of MT-A70 family proteins typically form heterodimers. For example, the m6A MTase core complex was a heterodimer of METTL3 and METTL14 (*42*), featuring METTL3 as the catalytic core and METTL14 with an eroded EPPL motif as the RNA binding platform (*43*). Similarly, in the 6mA maintenance MTase complex, the enzymatic activity of the DPPW-containing AMT1 (MTA1) required the DPPW-lacking AMT7, with AMT7 contributing to complex stabilization and DNA binding (*10*, *39*, *41*). In line with these reports, the predicted structure of MT-A70 domains in AMT2-AMT5 exhibited a notable similarity to those in METTL3-METTL14 and AMT1-AMT7 (MTA1-MTA9) (fig. S14A) (*40*–*42*, *44*), suggesting a heterodimer association of AMT2 and AMT5. However, the heterodimer formed by full-length AMT2 and AMT5 superimposed with the AMT1 complex only in their conserved MT-A70 domains, but not in AMTP1 and AMTP2 (fig. S14B), the latter of which are indispensable for the MTase activity of AMT1 complex (*10*, *32*). In vitro and in vivo MTase assays revealed no catalytic activity for AMT2 in combination with AMT5, strongly indicating that the de novo MTase complex requires additional components (fig. S9).

In addition, we also found homologs of AMT2 in the free-living excavate amoeba-flagellate *Naegleria gruberi* and the occasional disease-causing amoeba *Acanthamoeba castellanii* (Fig. 7B). It is tempting to speculate that undiscovered de novo 6mA methylation or even de novo DNA synthesis may be present in these two species.

Comparing 6mA and 5mC

There are several key similarities between de novo 6mA in the new MAC of *Tetrahymena* and de novo 5mC in the early embryogenesis of mammalian cells. First, both modifications occur during the transition from a zygotic nucleus to a somatic nucleus (*8*, *45*), accomplished by intensive epigenome reprogramming (*46*, *47*). Second, in both cases, de novo DNA methylation is catalyzed by specific DNA MTase(s), AMT2 and AMT5 in the case of 6mA and DNMT3A and DNMT3B for 5mC (*16*). Third, the de novo depositions of both 6mA and 5mC reply on a complex interplay with other epigenetic factors to establish specific patterns. For 6mA, active transcription marks such as H2A.Z and H3K4me3, and possibly histone acetylation, are the major players (*8*, *27*). Repressive marks such as H3K9me3 and H3K27me3 might also play a role to confine the territory of 6mA (*48*). For 5mC, the concerto playing with H3K9me2/me3, as well as histone deacetylase, confers its genome targeting and reinforces its silencing effects (*49*). Fourth, both modifications play essential roles for proper development. Loss of AMT2 and/or AMT5 reduces the progeny viability in *Tetrahymena*, while the absence of DNMT3A and DNMT3B results in aberrant gene expression and embryo lethality in mammals (*16*).

It is also important to note that, while there are shared features, the distinctions between 6mA in *Tetrahymena* and 5mC in mammals are substantial, arising from their unique evolutionary background and biological contexts. First, the *Tetrahymena* zygotic nucleus originates from the 6mA-free MIC (*26*, *29*), thus requiring no demethylation prior to de novo 6mA deposition. Conversely, genome-wide de novo 5mC deposition occurs in parallel or after the germline 5mC was erased by both passive and active demethylation (*50*). Second, the de novo MTases for 6mA and 5mC have distinct enzymatic features. AMT2 and AMT5 convert unmethylated adenines to hemi-6mA, while DNMT3A and DNMT3B generate both hemi- and full-5mC (*51*). Third, in a fully methylated *Tetrahymena* somatic genome, only ~2% of ApT is methylated (*8*, *21*), while 60 to 80% of CpG are methylated in mammalian somatic genomes (*52*). Fourth, 6mA is closely associated with active transcription, fulfilling its role, together with other epigenetic factors such as H2A.Z and H3K4me3 (*8*, *11*, *27*) to activate the somatic transcription, so that *Tetrahymena* could thrive as a single cell executing a variety of

functions such as feeding and mating. In contrast, 5mC is primarily linked with gene repression, preventing the expression of genes unnecessary in specific cell types, besides limiting transposable elements and repetitive sequences (*53*, *54*).

In summary, our work established a notable parallel between 6mA and 5mC: both feature palindrome motifs (AT versus CG), transmit in a semiconservative manner, and require a two-step methylation pathway. Considering the dichotomy of 6mA prevalence in unicellular eukaryotes versus 5mC in multicellular eukaryotes, our study offers unique insights into the evolutionary divergence among eukaryotes from the unique perspective of DNA methylation.

METHODS AND MATERIALS

Cell culture

Tetrahymena WT strains, SB210 and CU428, were obtained from the *Tetrahymena* Stock Center (http://tetrahymena.vet.cornell.edu). *AMT1* germline KO homozygous homokaryon strain was generated in our previous work (*8*). KO and tag strains used in this study, most of which were newly generated, are listed in table S5. Cells were grown in SPP [1% protease peptone, 0.2% dextrose anhydrous, 0.1% yeast extract, 0.003% ethylenediaminetetraacetic acid (EDTA) ferric sodium salt] medium at 30°C (*55*).

Generation of *Tetrahymena* strains

Primers used in strain generation and confirmation are listed in table S6. To generate KO constructs, *neo4* or *bsr2* cassettes (*56*, *57*) were flanked with 5′ and 3′ flanking regions of *AMT2* (TTHERM_00388490) and *AMT5* (TTHERM_00136470) (fig. S1A). *AMT2* and/or *AMT5* germline single KO homozygous homokaryons and homozygous heterokaryons (Δ*AMT2* and Δ*AMT5*) were generated in our previous work (*8*). Germline double KO homozygous homokaryon and homozygous heterokaryon (Δ*AMT2*/*5*) were generated by crossing two mating types of homozygous heterokaryon Δ*AMT2* and Δ*AMT5* single KO cells (fig. S1, B and C). Somatic KO strains were generated as previously reported (fig. S1B) (*58*).

To generate tagging constructs, sequences coding for the HA tag were inserted to the C terminus of AMT2 or the N terminus of AMT5 and AMT1 (fig. S4A). Germline tagging strain of *AMT2* (*AMT2*-CHA) and somatic tagging strain of AMT5 (*AMT5*-NHA) were generated as previously reported (fig. S4B) (*8*). Germline tagging strain of *AMT1*-NHA in the background of WT cells (SB210 and CU428) was previously generated (*59*), while those in the background of *AMT2* and/or *AMT5* KO cells were generated by crossing two different mating types of homozygous heterokaryon *AMT1*-NHA with homozygous heterokaryons deleting each or both of *AMT2* and *AMT5* following the same strategy used for generating double KO cells (fig. S1B).

To generate *AMT2*-rescue (*AMT2*-RS) and *AMT5*-rescue (*AMT5*-RS) constructs, the full-length *AMT2* or *AMT5* ORF and its flanking regions were cloned and the *bsr2* cassette was inserted into the 3′ untranslated region. DNA sequences coding for the HA tag were inserted to the C terminus of AMT2 or the N terminus of AMT5. The rescue construct was transformed into the MAC of corresponding germline KO cells and selected by blasticidin S (fig. S5).

To generate *AMT2* mutants, a sequence spanning the 5′ flanking region, the full-length *AMT2* with a C-terminal HA tag, the 3′ flanking region, and the *bsr2* cassette was polymerase chain reaction (PCR) amplified from the somatic *AMT2*-RS cells. The APPA mutation was introduced by fusion PCR with primers containing the designed mutations (table S6). The *AMT2*-APPA or *AMT2*-APPF construct was transformed into the somatic MAC of Δ*AMT2* cells and selected by blasticidin S (fig. S5, A to D). To distinguish true progeny from quitter, the *RPB3*-CHA-bsr2 construct with a HA tag at the C terminus of RPB3 was transformed into the somatic MAC of WT, Δ*AMT2*, Δ*AMT5*, and Δ*AMT2/5* cells (Fig. 6E and fig. S7A).

IF staining

Different fixation methods using 2% paraformaldehyde (Sigma-Aldrich, P6148), combination of saturated $HgCl_2$ (HQ, HG 3-1068-77) and ethanol (1:2), or 10% formalin (Nacalai Tesque, 16223-55) were used as previously described (*8*, *27*, *34*, *58*). Conjugative cells were fixed at indicated time points after mixing cells of two different mating types. The primary antibodies were α-6mA (Synaptic Systems, 202003; 1:2000; rabbit), α-HA (Cell Signaling Technology, C29F4; 1:200; rabbit), and α-HA (Covance, MMS-101P; 1:500; mouse). The secondary antibodies were goat anti-rabbit immunoglobulin G (IgG; H+L), Alexa Fluor 555 (Invitrogen, A-21428; 1:4000); goat anti-rabbit IgG (H+L), Alexa Fluor 546 (Invitrogen, A-11035; 1:4000); and goat anti-mouse IgG (H+L), Alexa Fluor 488 (Invitrogen, A-11001; 1:4000).

Purification of new MACs

The new MACs were isolated from conjugative WT and KO cells by differential centrifugation following previous procedures (*60*). Briefly, nuclear pellets containing a large proportion of new MACs were collected at 3500 to 4500 g from 24 hours post-mixing cells. Nuclear pellets were washed once with 4′,6-diamidino-2-phenylindol (DAPI) (Roche, 10236276001) in methanol (1 μg/ml), then resuspended in DAPI-methanol (1 μg/ml), and incubated in the dark at room temperature for 15 min. Nuclei were resuspended in modified TMSN buffer [0.25 M sucrose, 10 mM tris-HCl (pH 7.5), 3 mM $CaCl_2$, 0.016% NP-40, and 1× EDTA-free protease inhibitor cocktail (Roche, 11873580001)] (*34*) and sorted by Becton Dickinson FACSAria III flow cytometer (Becton, Dickinson and Company, Pleasanton, CA, USA). The purity of the collected new MACs was assessed by DAPI-stained nuclear morphology. MICs were easily distinguished by their much smaller size; somatic MACs and new MACs were distinguishable by their differences in size (bigger versus smaller) and DAPI signal intensity (stronger versus weaker). Contamination rate of somatic MACs and MICs in the new MAC fraction was <2 and <10%, respectively.

UHPLC-QQQ-MS/MS analysis

Genomic DNA was extracted using DNA Extraction Reagent (Solarbio, P1012) or QIAGEN Genomic-tip 20/G (10223) and then processed into single nucleotides as previously described (*8*). These single nucleotides were analyzed by ultrahigh-performance liquid chromatography–tandem MS (UHPLC-QQQ-MS/MS) on an Acquity BEH C18 column (100 mm by 2.1 mm, 1.7 μm, Waters, MA, USA) using a Xevo TQ-S triple quadrupole mass spectrometer (Waters, Milford, MA, USA) or a Hypersil GOLD column (100 mm by 2.1 mm, 1.9 μm, Thermo Fisher Scientific) using a TSQ Quantiva mass spectrometer (Thermo Fisher Scientific). The mass spectrometer was set to multiple reaction monitoring (MRM) under positive electrospray mode. For 6mA and A, the selective MRM transitions were detected under mass/charge ratio (*m*/*z*) 266/150 and *m*/*z* 252/136, respectively. The ratio of 6mA/A was quantified

by the running nucleoside standards calibration curves at the same time.

Conjugation progress analysis and viability test

To monitor the conjugation progress, cells at different stages (4, 6, 10, 14, and 24 hours after mixing) of Δ*AMT2* (mating types IV and V), Δ*AMT5* (mating types II and IV), Δ*AMT2*/Δ*AMT5* (mating types II and IV), and WT (SB210 and CU428) were fixed with 2% paraformaldehyde, stained with DAPI (1 μg/ml; Bio Basic, Inc., E607303), and observed under the microscope.

For the viability test of each KO strain (WT cells were used as the control), individual mating pair was picked into SPP medium drops at 10 hours post-mixing. After 2 to 3 days of culture, cells were transferred into 96-well plates. It should be noted that the blasticidin S resistance was introduced into the parental MAC of mating cells by transforming a *bsr2* cassette–containing construct (*57*), which could help to distinguish true progenies (blasticidin S sensitive) from aborted pairs (quitters, blasticidin S resistant) (fig. S7A). Viable cells in 96-well plates that were sensitive to blasticidin S were counted as viable true progenies. True progenies had mating types other than that of parental cells, demonstrated by PCR amplification–based test using mating type primers (fig. S7B and table S6) (*61*), confirming the efficacy of blasticidin S selection.

SMRT sequencing and data analysis

Genomic DNA was extracted from fluorescence-activated cell sorting–sorted new MACs of both WT and KO cells using DNA Extraction Reagent (Solarbio, P1012). The quality and concentration of DNA were assessed by agarose gel electrophoresis and the Qubit3.0 Fluorometer (Thermo Fisher Scientific).

Sample preparation and data analysis followed the latest SMRT CCS analysis pipeline (*21*, *62*). Genomic DNA was sheared to approximately 3 kb to generate PacBio Sequel II libraries, ensuring sufficient genomic coverage and subreads sequencing depth. To evaluate the sequencing quality, SAMtools (*63*) was used to sort the subreads, and the ccs module (SMRT Link v11.0, Pacific Biosciences) was used to generate circular consensus sequence and sequencing information for each single molecule. Custom Perl scripts were then used to extract high-confidence single molecules (passes ≥ 30×) for downstream analyses.

Single molecules were mapped to their corresponding consensus sequence using BLASR (*64*), and IPD (interpulse duration) ratios were calculated using ipdSummary (SMRT Link v11.0, Pacific Biosciences). Single molecules with global dispersion, defined as large IPD ratio SD in Watson and/or Crick strands (SD ≥ 0.35) for all unmethylated adenine sites (IPD ratios < 2.8), were filtered out. To minimize the impact of sequencing variability, single molecules with local dispersion of IPD ratios, characterized by high-density of N*, were filtered out (*21*).

Circular consensus sequences of selected single molecules were mapped back to the *Tetrahymena* genome assembly, which contained sequences from the MIC, MAC, and mitochondrion genomes (*65*–*68*), using blastn (*69*) with the parameter "-max_hsps 1, -max_target_seqs 1." MAC-mapped reads (mapped length ≥ 95% for read length and mapped identity ≥ 98%) were selected for further analysis. Potential MIC reads contaminations were detected on the basis of the alignment score difference between MIC and MAC (Δ ≥ 50) (*21*). 6mA IPD ratio threshold of all single molecules were calculated by applying the bimodal distribution deconvolution to IPD ratios.

RNA sequencing and data analysis

Progenies of Δ*AMT2* (mating types IV and V), Δ*AMT5* (mating types II and IV), Δ*AMT2/5* (mating types II and IV), and WT (SB210 and CU428) cells were distinguished from non-maters and quitters on the basis of their resistance to blasticidin S (fig. S7A). Total RNA from two replicates of each strain was extracted at about 20 generations after refeeding using RNAiso Plus (Takara, 9108).

After trimming sequencing adapters and filtering out low quality reads by Trim Galore (*70*), the resulting paired reads were mapped to the latest MAC genome assembly in the *Tetrahymena* genome database (TGD) (http://ciliate.org) (*65*, *68*) using HISAT2 (*71*). Discordant alignments for paired reads were discarded. Only paired reads with unique mapping, as indicated by the presence of the "NH:i:1" tag in the mapped SAM file, were retained. PCR duplicates were removed using the Picard MarkDuplicates tool (http://broadinstitute.github.io/picard/). The featureCounts program (*72*) was used for counting reads mapped to genomic features, using gene annotation file from TGD as the reference. The average reads for each gene in every strain were calculated to elucidate the similarity of transcription profiles. The Spearman's correlation coefficient between every two strains was calculated using R, and the heatmap was generated using the gplots package (*73*).

Phylogenetic tree construction

The amino acid sequences of AMT2 and AMT5 were queried against the protein databases of selected species (file S1) using PSI-BLAST (*74*). Sequences with an *E*-value below 10^{-4} were selected for phylogenetic tree construction and aligned using the MAFFT program (*75*). IQ-TREE2 was used to generate the phylogenetic tree using the approximate maximum-likelihood method with 1000 replicates for ultrafast bootstrap (*76*, *77*). Proteins used for phylogenetic analysis are listed in file S1, while sequences of some unpublished proteins were provided in file S2.

Supplementary Materials

This PDF file includes:

Supplementary Methods
Figs. S1 to S14
Tables S1 to S6
Files S1 and S2
References

REFERENCES AND NOTES

1. Y. Fu, G. Luo, K. Chen, X. Deng, M. Yu, D. Han, Z. Hao, J. Liu, X. Lu, L. C. Dore, X. Weng, Q. Ji, L. Mets, C. He, N^6-methyldeoxyadenosine marks active transcription start sites in *Chlamydomonas*. *Cell* **161**, 879–892 (2015).
2. E. L. Greer, M. A. Blanco, L. Gu, E. Sendinc, J. Liu, D. Aristizábal-Corrales, C. Hsu, L. Aravind, C. He, Y. Shi, DNA methylation on N^6-adenine in *C. elegans*. *Cell* **161**, 868–878 (2015).
3. G. Zhang, H. Huang, D. Liu, Y. Cheng, X. Liu, W. Zhang, R. Yin, D. Zhang, P. Zhang, J. Liu, C. Li, B. Liu, Y. Luo, Y. Zhu, N. Zhang, S. He, C. He, H. Wang, D. Chen, N^6-methyladenine DNA modification in *Drosophila*. *Cell* **161**, 893–906 (2015).
4. M. Zhang, S. Yang, R. Nelakanti, W. Zhao, G. Liu, Z. Li, X. Liu, T. Wu, A. Xiao, H. Li, Mammalian ALKBH1 serves as an N^6-mA demethylase of unpairing DNA. *Cell Res.* **30**, 197–210 (2020).
5. T. P. Wu, T. Wang, M. G. Seetin, Y. Lai, S. Zhu, K. Lin, Y. Liu, S. D. Byrum, S. G. Mackintosh, M. Zhong, A. Tackett, G. Wang, L. S. Hon, G. Fang, J. A. Swenberg, A. Z. Xiao, DNA methylation on N^6-adenine in mammalian embryonic stem cells. *Nature* **532**, 329–333 (2016).
6. S. Zhang, B. Li, K. Du, T. Liang, M. Dai, W. Huang, H. Zhang, Y. Ling, H. Zhang, Epigenetically modified N^6-methyladenine inhibits DNA replication by human DNA polymerase iota. *Biochimie* **168**, 134–143 (2020).
7. X. Zhang, R. M. Blumenthal, X. Cheng, A role for N^6-methyladenine in DNA damage repair. *Trends Biochem. Sci.* **46**, 175–183 (2021).

8. Y. Wang, Y. Sheng, Y. Liu, W. Zhang, T. Cheng, L. Duan, B. Pan, Y. Qiao, Y. Liu, S. Gao, A distinct class of eukaryotic MT-A70 methyltransferases maintain symmetric DNA N^6-adenine methylation at the ApT dinucleotides as an epigenetic mark associated with transcription. *Nucleic Acids Res.* **47**, 11771–11789 (2019).
9. B. Pan, F. Ye, T. Li, F. Wei, A. Warren, Y. Wang, S. Gao, Potential role of N^6-adenine DNA methylation in alternative splicing and endosymbiosis in *Paramecium bursaria*. *iScience* **26**, 106676 (2023).
10. L. Y. Beh, G. T. Debelouchina, D. M. Clay, R. E. Thompson, K. A. Lindblad, E. R. Hutton, J. R. Bracht, R. P. Sebra, T. W. Muir, L. F. Landweber, Identification of a DNA N^6-adenine methyltransferase complex and its impact on chromatin organization. *Cell* **177**, 1781–1796.e25 (2019).
11. C. Ma, R. Niu, T. Huang, L. W. Shao, Y. Peng, W. Ding, Y. Wang, G. Jia, C. He, C. Y. Li, A. He, Y. Liu, N^6-methyldeoxyadenine is a transgenerational epigenetic signal for mitochondrial stress adaptation. *Nat. Cell Biol.* **21**, 319–327 (2019).
12. B. Yao, Y. Cheng, Z. Wang, Y. Li, L. Chen, L. Huang, W. Zhang, D. Chen, H. Wu, B. Tang, P. Jin, DNA N^6-methyladenine is dynamically regulated in the mouse brain following environmental stress. *Nat. Commun.* **8**, 1122 (2017).
13. J. Liu, Y. Zhu, G. Luo, X. Wang, Y. Yue, X. Wang, X. Zong, K. Chen, H. Yin, Y. Fu, D. Han, Y. Wang, D. Chen, C. He, Abundant DNA 6mA methylation during early embryogenesis of zebrafish and pig. *Nat. Commun.* **7**, 13052 (2016).
14. Z. Liang, L. Shen, X. Cui, S. Bao, Y. Geng, G. Yu, F. Liang, S. Xie, T. Lu, X. Gu, H. Yu, DNA N^6-adenine methylation in *Arabidopsis thaliana*. *Dev. Cell* **45**, 406–416.e3 (2018).
15. Q. Xie, T. P. Wu, R. C. Gimple, Z. Li, B. C. Prager, Q. Wu, Y. Yu, P. Wang, Y. Wang, D. U. Gorkin, C. Zhang, A. V. Dowiak, K. Lin, C. Zeng, Y. Sui, L. J. Y. Kim, T. E. Miller, L. Jiang, C. Lee-Poturalski, Z. Huang, X. Fang, K. Zhai, S. C. Mack, M. Sander, S. Bao, A. E. Kerstetter-Fogle, A. E. Sloan, A. Z. Xiao, J. N. Rich, N^6-methyladenine DNA modification in glioblastoma. *Cell* **175**, 1228–1243.e20 (2018).
16. M. Okano, D. Bell, D. Haber, E. Li, DNA methyltransferases Dnmt3a and Dnmt3b are essential for *de novo* methylation and mammalian development. *Cell* **99**, 247–257 (1999).
17. J. A. Yoder, N. S. Soman, G. L. Verdine, T. H. Bestor, DNA (cytosine-5)-methyltransferases in mouse cells and tissues. Studies with a mechanism-based probe. *J. Mol. Biol.* **270**, 385–395 (1997).
18. R. Stein, Y. Gruenbaum, Y. Pollack, A. Razin, H. Cedar, Clonal inheritance of the pattern of DNA methylation in mouse cells. *Proc. Natl. Acad. Sci. U.S.A.* **79**, 61–65 (1982).
19. T. Kafri, M. Ariel, M. Brandeis, R. Shemer, L. Urven, J. Mccarrey, H. Cedar, A. Razin, Developmental pattern of gene-specific DNA methylation in the mouse embryo and germ line. *Genes Dev.* **6**, 705–714 (1992).
20. L. Zhao, F. Gao, S. Gao, Y. Liang, H. Long, Z. Lyu, Y. Su, N. Ye, L. Zhang, C. Zhao, X. Wang, W. Song, S. Zhang, B. Dong, Biodiversity-based development and evolution: The emerging research systems in model and non-model organisms. *Sci. China Life Sci.* **64**, 1236–1280 (2021).
21. Y. Sheng, Y. Wang, W. Yang, X. Q. Wang, J. Lu, B. Pan, B. Nan, Y. Liu, C. Li, J. Song, Y. Dou, S. Gao, Y. Liu, Semi-conservative transmission of DNA N^6-adenine methylation in a unicellular eukaryote. *Genome Res.* **34**, 740–756 (2024).
22. M. Bochtler, H. Fernandes, DNA adenine methylation in eukaryotes: Enzymatic mark or a form of DNA damage? *Bioessays* **43**, e2000243 (2021).
23. K. M. Karrer, Nuclear dualism. *Methods Cell Biol.* **109**, 29–52 (2012).
24. F. Wei, B. Pan, J. Diao, Y. Wang, Y. Sheng, S. Gao, The micronuclear histone H3 clipping in the unicellular eukaryote *Tetrahymena thermophila*. *Mar. Life Sci. Technol.* **4**, 584–594 (2022).
25. M. Tian, X. Cai, Y. Liu, M. Liucong, R. Howard-Till, A practical reference for studying meiosis in the model ciliate *Tetrahymena thermophila*. *Mar. Life Sci. Technol.* **4**, 595–608 (2022).
26. M. A. Gorovsky, H. Pleger, [^{6}N]methyl adenine in the nuclear DNA of a eucaryote, *Tetrahymena pyriformis*. *J. Mol. Biol.* **56**, 697–701 (1973).
27. Y. Wang, X. Chen, Y. Sheng, Y. Liu, S. Gao, N^6-adenine DNA methylation is associated with the linker DNA of H2A.Z-containing well-positioned nucleosomes in Pol II-transcribed genes in *Tetrahymena*. *Nucleic Acids Res.* **45**, 11594–11606 (2017).
28. S. J. Mondo, R. O. Dannebaum, R. C. Kuo, K. B. Louie, A. J. Bewick, K. LaButti, S. Haridas, A. Kuo, A. Salamov, S. R. Ahrendt, R. Lau, B. P. Bowen, A. Lipzen, W. Sullivan, B. B. Andreopoulos, A. Clum, E. Lindquist, C. Daum, T. R. Northen, G. Kunde-Ramamoorthy, R. J. Schmitz, A. Gryganskyi, D. Culley, J. Magnuson, T. Y. James, M. A. O'Malley, J. E. Stajich, J. W. Spatafora, A. Visel, I. V. Grigoriev, Widespread adenine N^6-methylation of active genes in fungi. *Nat. Genet.* **49**, 964–968 (2017).
29. G. S. Harrison, K. M. Karrer, DNA synthesis, methylation and degradation during conjugation in *Tetrahymena thermophila*. *Nucleic Acids Res.* **13**, 73–87 (1985).
30. W. Miao, J. Xiong, J. Bowen, W. Wang, Y. Liu, O. Braguinets, J. Grigull, R. E. Pearlman, E. Orias, M. A. Gorovsky, Microarray analyses of gene expression during the *Tetrahymena thermophila* life cycle. *PLOS One* **4**, e4429 (2009).
31. L. M. Iyer, D. Zhang, L. Aravind, Adenine methylation in eukaryotes: Apprehending the complex evolutionary history and functional potential of an epigenetic modification. *Bioessays* **38**, 27–40 (2016).
32. Y. Wang, B. Nan, F. Ye, Z. Zhang, W. Yang, B. Pan, F. Wei, L. Duan, H. Li, J. Niu, A. Ju, Y. Liu, D. Wang, W. Zhang, Y. Liu, S. Gao, Dual modes of DNA N^6-methyladenine maintenance by distinct methyltransferase complexes. *Proc. Natl. Acad. Sci. U.S.A.* **122**, e2413037121 (2025).
33. L. A. Stargell, J. Bowen, C. A. Dadd, P. C. Dedon, M. Davis, R. G. Cook, C. D. Allis, M. A. Gorovsky, Temporal and spatial association of histone H2A variant hv1 with transcriptionally competent chromatin during nuclear development in *Tetrahymena thermophila*. *Genes Dev.* **7**, 2641–2651 (1993).
34. K. Kataoka, K. Mochizuki, Phosphorylation of an HP1-like protein regulates heterochromatin body assembly for DNA elimination. *Dev. Cell* **35**, 775–788 (2015).
35. C. D. Allis, M. Colavito-Shepanski, M. A. Gorovsky, Scheduled and unscheduled DNA synthesis during development in conjugating *Tetrahymena*. *Dev. Biol.* **124**, 469–480 (1987).
36. B. B. McDonald, Synthesis of deoxyribonucleic acid by micro- and macronuclei of *Tetrahymena pyriformis*. *J. Cell Biol.* **13**, 193–203 (1962).
37. D. H. Lynn, *The Ciliated Protozoa: Characterization, Classification, and Guide to the Literature* (Springer Science and Business Media B.V., ed. 3, 2008).
38. J. Xiong, W. Yang, K. Chen, C. Jiang, W. Miao, Hidden genomic evolution in a morphospecies-The landscape of rapidly evolving genes in *Tetrahymena*. *PLoS Biol.* **17**, e3000294 (2019).
39. J. Chen, R. Hu, Y. Chen, X. Lin, W. Xiang, H. Chen, C. Yao, L. Liu, Structural basis for MTA1c-mediated DNA N^6-adenine methylation. *Nat. Commun.* **13**, 3257 (2022).
40. C. B. Woodcock, J. R. Horton, X. Zhang, R. M. Blumenthal, X. Cheng, Beta class amino methyltransferases from bacteria to humans: Evolution and structural consequences. *Nucleic Acids Res.* **48**, 10034–10044 (2020).
41. J. Yan, F. Liu, Z. Guan, X. Yan, X. Jin, Q. Wang, Z. Wang, J. Yan, D. Zhang, Z. Liu, Structural insights into DNA N^6-adenine methylation by the MTA1 complex. *Cell Discov.* **9**, 8 (2023).
42. J. Liu, Y. Yue, D. Han, X. Wang, Y. Fu, L. Zhang, G. Jia, M. Yu, Z. Lu, X. Deng, A METTL3-METTL14 complex mediates mammalian nuclear RNA N^6-adenosine methylation. *Nat. Chem. Biol.* **10**, 93–95 (2014).
43. P. Wang, K. A. Doxtader, Y. Nam, Structural basis for cooperative function of Mettl3 and Mettl14 methyltransferases. *Mol. Cell* **63**, 306–317 (2016).
44. J. Abramson, J. Adler, J. Dunger, R. Evans, T. Green, A. Pritzel, O. Ronneberger, L. Willmore, A. J. Ballard, J. Bambrick, S. W. Bodenstein, D. A. Evans, C.-C. Hung, M. O'Neill, D. Reiman, K. Tunyasuvunakool, Z. Wu, A. Žemgulytė, E. Arvaniti, C. Beattie, O. Bertolli, A. Bridgland, A. Cherepanov, M. Congreve, A. I. Cowen-Rivers, A. Cowie, M. Figurnov, F. B. Fuchs, H. Gladman, R. Jain, Y. A. Khan, C. M. R. Low, K. Perlin, A. Potapenko, P. Savy, S. Singh, A. Stecula, A. Thillaisundaram, C. Tong, S. Yakneen, E. D. Zhong, M. Zielinski, A. Žídek, V. Bapst, P. Kohli, M. Jaderberg, D. Hassabis, J. M. Jumper, Accurate structure prediction of biomolecular interactions with AlphaFold 3. *Nature* **630**, 493–500 (2024).
45. L. Li, X. Lu, J. Dean, The maternal to zygotic transition in mammals. *Mol. Aspects Med.* **34**, 919–938 (2013).
46. W. Reik, W. Dean, J. Walter, Epigenetic reprogramming in mammalian development. *Science* **293**, 1089–1093 (2001).
47. E. Meyer, S. Duharcourt, Epigenetic programming of developmental genome rearrangements in ciliates. *Cell* **87**, 9–12 (1996).
48. J. H. Suhren, T. Noto, K. Kataoka, S. Gao, Y. Liu, K. Mochizuki, Negative regulators of an RNAi-heterochromatin positive feedback loop safeguard somatic genome integrity in *Tetrahymena*. *Cell Rep.* **18**, 2494–2507 (2017).
49. B. Lehnertz, Y. Ueda, A. A. Derijck, U. Braunschweig, L. Perez-Burgos, S. Kubicek, T. Chen, E. Li, T. Jenuwein, A. H. Peters, Suv39h-mediated histone H3 lysine 9 methylation directs DNA methylation to major satellite repeats at pericentric heterochromatin. *Curr. Biol.* **13**, 1192–1200 (2003).
50. R. M. Kohli, Y. Zhang, TET enzymes, TDG and the dynamics of DNA demethylation. *Nature* **502**, 472–479 (2013).
51. C. L. Hsieh, The *de novo* methylation activity of Dnmt3a is distinctly different than that of Dnmt1. *BMC Biochem.* **6**, 6 (2005).
52. Z. D. Smith, A. Meissner, DNA methylation: Roles in mammalian development. *Nat. Rev. Genet.* **14**, 204–220 (2013).
53. M. Kim, Y. K. Park, T. W. Kang, S. H. Lee, Y. H. Rhee, J. L. Park, H. J. Kim, D. Lee, D. Lee, S. Y. Kim, Y. S. Kim, Dynamic changes in DNA methylation and hydroxymethylation when hES cells undergo differentiation toward a neuronal lineage. *Hum. Mol. Genet.* **23**, 657–667 (2014).
54. Ö. Deniz, J. M. Frost, M. R. Branco, Regulation of transposable elements by DNA modifications. *Nat. Rev. Genet.* **20**, 417–431 (2019).
55. M. Sweet, C. D. Allis, *Cells: A Laboratory Manual*, D. L. Spector, R. D. Goldman, L. A. Leinwand, Eds. (Cold Spring Harbor Laboratory Press, 1998), vol. 1.
56. K. Mochizuki, High efficiency transformation of *Tetrahymena* using a codon-optimized neomycin resistance gene. *Gene* **425**, 79–83 (2008).
57. K. B. Talsky, K. Collins, Strand-asymmetric endogenous *Tetrahymena* small RNA production requires a previously uncharacterized uridylyltransferase protein partner. *RNA* **18**, 1553–1562 (2012).

58. S. Gao, J. Xiong, C. Zhang, B. R. Berquist, R. Yang, M. Zhao, A. J. Molascon, S. Y. Kwiatkowsk, D. Yuan, Z. Qin, J. Wen, G. M. Kapler, P. C. Andrews, W. Miao, Y. Liu, Impaired replication elongation in *Tetrahymena* mutants deficient in histone H3 Lys 27 monomethylation. *Genes Dev.* **27**, 1662–1679 (2013).
59. L. Duan, H. Li, A. Ju, Z. Zhang, J. Niu, Y. Zhang, J. Diao, K. Kataoka, H. Ma, N. Song, S. Gao, Y. Wang, Methyl-dependent auto-regulation of the DNA N^6-adenine methyltransferase AMT1 in the unicellular eukaryote *Tetrahymena thermophila*. *Nucleic Acids Res.* **53**, gkaf022 (2025).
60. L. Feng, G. Wang, E. P. Hamilton, J. Xiong, G. Yan, K. Chen, X. Chen, W. Dui, A. Plemens, L. Khadr, A. Dhanekula, M. Juma, H. Q. Dang, G. M. Kapler, E. Orias, W. Miao, Y. Liu, A germline-limited piggyBac transposase gene is required for precise excision in *Tetrahymena* genome rearrangement. *Nucleic Acids Res.* **45**, 9481–9502 (2017).
61. M. D. Cervantes, E. P. Hamilton, J. Xiong, M. J. Lawson, D. Yuan, M. Hadjithomas, W. Miao, E. Orias, M. D. Cervantes, E. P. Hamilton, Selecting one of several mating types through gene segment joining and deletion in *Tetrahymena thermophila*. *PLoS Biol.* **11**, e1002284 (2013).
62. H. Li, J. Niu, Y. Sheng, Y. Liu, S. Gao, SMAC: Identifying DNA N^6-methyladenine (6mA) at the single-molecule level using SMRT CCS data. *Brief. Bioinform.* **26**, bbaf153 (2025).
63. H. Li, B. Handsaker, A. Wysoker, T. Fennell, J. Ruan, N. Homer, G. Marth, G. Abecasis, R. Durbin, G. P. D. P. Subgroup, The sequence alignment/map format and SAMtools. *Bioinformatics* **25**, 2078–2079 (2009).
64. M. J. Chaisson, G. Tesler, Mapping single molecule sequencing reads using basic local alignment with successive refinement (BLASR): Application and theory. *BMC bioinformatics* **13**, 238 (2012).
65. Y. Sheng, L. Duan, T. Cheng, Y. Qiao, N. A. Stover, S. Gao, The completed macronuclear genome of a model ciliate *Tetrahymena thermophila* and its application in genome scrambling and copy number analyses. *Sci. China Life Sci.* **63**, 1534–1542 (2020).
66. G. Burger, Y. Zhu, T. G. Littlejohn, S. J. Greenwood, M. N. Schnare, B. F. Lang, M. W. Gray, Complete sequence of the mitochondrial genome of *Tetrahymena pyriformis* and comparison with *Paramecium aurelia* mitochondrial DNA. *J. Mol. Biol.* **297**, 365–380 (2000).
67. E. P. Hamilton, A. Kapusta, P. E. Huvos, S. L. Bidwell, N. Zafar, H. Tang, M. Hadjithomas, V. Krishnakumar, J. H. Badger, E. V. Caler, Structure of the germline genome of *Tetrahymena thermophila* and relationship to the massively rearranged somatic genome. *eLife* **5**, e19090 (2016).
68. F. Ye, X. Chen, Y. Li, A. Ju, Y. Sheng, L. Duan, J. Zhang, Z. Zhang, K. A. S. Al-Rasheid, N. A. Stover, S. Gao, Comprehensive genome annotation of the model ciliate *Tetrahymena thermophila* by in-depth epigenetic and transcriptomic profiling. *Nucleic Acids Res.* **53**, gkae1177 (2025).
69. J. Ye, S. McGinnis, T. L. Madden, BLAST: Improvements for better sequence analysis. *Nucleic Acids Res.* **34**, W6–W9 (2006).
70. F. Krueger, F. James, P. Ewels, E. Afyounian, B. Schuster-Boeckler, FelixKrueger/TrimGalore: v0. 6.7-DOI via Zenodo, version 0.6.7, Zenodo (2021); https://zenodo.org/record/5127899#.YytIuC0RpQI.
71. D. Kim, J. M. Paggi, C. Park, C. Bennett, S. L. Salzberg, Graph-based genome alignment and genotyping with HISAT2 and HISAT-genotype. *Nat. Biotechnol.* **37**, 907–915 (2019).
72. Y. Liao, G. K. Smyth, W. Shi, featureCounts: An efficient general purpose program for assigning sequence reads to genomic features. *Bioinformatics* **30**, 923–930 (2014).
73. G. R. Warnes, B. M. Bolker, L. Bonebakker, R. Gentleman, W. Liaw, T. Lumley, M. Maechler, A. Magnusson, S. Moeller, M. L. Schwartz, B. A. B. Venables, W. Huber, A. Liaw, R. Gregory, B. Warnes, L. Bonebakker, W. H. A. Liaw, T. Lumley, M. Maechler, A. Magnusson, S. Moeller, M. Schwartz, B. A. B. Venables, Gplots: Various R programming tools for plotting data, version 2.17.0, R Package (2015); http://cran.r-project.org/package=gplots.
74. A. A. Schaffer, L. Aravind, T. L. Madden, S. Shavirin, J. L. Spouge, Y. I. Wolf, E. V. Koonin, S. F. Altschul, Improving the accuracy of PSI-BLAST protein database searches with composition-based statistics and other refinements. *Nucleic Acids Res.* **29**, 2994–3005 (2001).
75. K. Katoh, K. Misawa, K. Kuma, T. Miyata, MAFFT: A novel method for rapid multiple sequence alignment based on fast Fourier transform. *Nucleic Acids Res.* **30**, 3059–3066 (2002).
76. D. T. Hoang, O. Chernomor, A. von Haeseler, B. Q. Minh, L. S. Vinh, UFBoot2: Improving the ultrafast bootstrap approximation. *Mol. Biol. Evol.* **35**, 518–522 (2018).
77. B. Q. Minh, H. A. Schmidt, O. Chernomor, D. Schrempf, M. D. Woodhams, A. von Haeseler, R. Lanfear, IQ-TREE 2: New models and efficient methods for phylogenetic inference in the genomic era. *Mol. Biol. Evol.* **37**, 1530–1534 (2020).
78. G. Z. Luo, Z. Hao, L. Luo, M. Shen, D. Sparvoli, Y. Zheng, Z. Zhang, X. Weng, K. Chen, Q. Cui, A. P. Turkewitz, C. He, N^6-methyldeoxyadenosine directs nucleosome positioning in *Tetrahymena* DNA. *Genome Biol.* **19**, 200 (2018).
79. Z. Zhou, C. Li, Q. Yuan, Y. Chi, Y. Li, Y. Yan, S. A. Al-Farraj, N. A. Stover, Z. Chen, X. Chen, Single-cell transcriptomic analysis reveals genome evolution in predatory litostomatean ciliates. *Eur. J. Protistol.* **93**, 126062 (2024).
80. Y. Liu, J. Niu, F. Ye, T. Solberg, B. Lu, C. Wang, M. Nowacki, S. Gao, Dynamic DNA N^6-adenine methylation (6mA) governs the encystment process, showcased in the unicellular eukaryote *Pseudocohnilembus persalinus*. *Genome Res.* **34**, 256–271 (2024).

Acknowledgments: We would like to thank the following people for assistance with this study: Y. Liu (University of Southern California, USA), Z. Lyu [Ocean University of China (OUC), China], and members of the Gao laboratory for fruitful discussion; K. Liu (Wuhan University, China) for suggestions on protein purification; C. Li, L. Lyu, R. Wang, and Y. Li (OUC) for providing their unpublished genomic data of multiple ciliates (file S2); J. Shi and Y. Zhang (OUC) for assisting the flow cytometry sorting; N. Song for assisting the MS analysis; and Y. Matsuda and H. Iinuma for assisting the radioactive experiments (Radioisotope Center of the National Institute for Basic Biology). High-performance computing resources for data processing were provided by the Institute of Evolution and Marine Biodiversity at OUC, the Center for High Performance Computing and System Simulation at Laoshan Laboratory, and Marine Big Data Center of Institute for Advanced Ocean Study at OUC. Our special thanks are given to W. Song (OUC) for helpful suggestions during drafting the manuscript. **Funding:** This work is supported by the National Natural Science Foundation of China (32125006 to S.G.), Natural Science Foundation of Shandong Province of China (ZR2024ZD40 to S.G.), the Science and Technology Innovation Project of Laoshan Laboratory (LSKJ202203203 to S.G.), JSPS KAKENHI Grants (17H07334, 18H02423, 22 K06186, and 22H05607 to K.K.), and JSPS KAKENHI Grants (JP24H02324 to J.Na.). **Author contributions:** T.C.: Conceptualization, investigation, validation, visualization, methodology, data curation, writing—original draft, and writing—review and editing. J.Z. and J.D.: Investigation, validation, visualization, methodology, data curation, writing—original draft, and writing—review and editing. H.L.: Investigation, software, data curation, validation, visualization, methodology, and writing—review and editing. W.Z. and J.Ni.: Investigation. J.Na.: Funding acquisition and supervision. T.K.: Methodology. K.K.: Conceptualization, funding acquisition, supervision, methodology, resources, visualization, and writing—review and editing. S.G.: Conceptualization, supervision, project administration, funding acquisition, methodology, resources, visualization, writing—original draft, and writing—review and editing. **Competing interests:** The authors declare that they have no competing interests. **Data and materials availability:** All data needed to evaluate the conclusions in the paper are present in the paper and/or the Supplementary Materials. The latest SB210 MAC genome can be found at the TGD (http://ciliate.org). RNA-sequencing data used in this study were deposited at the National Center for Biotechnology Information (NCBI) database (PRJNA1071335). SMRT CCS analysis results and scripts were uploaded to https://doi.org/10.5281/zenodo.14194932 (these data are also available at https://github.com/liiihc/CCS-analysis-results-and-scripts.git).

Submitted 15 May 2024
Accepted 14 April 2025
Published 14 May 2025
10.1126/sciadv.adq4623